TIME AND SPACE DEVELOPMENT OF ANISOTROPY IN A SPANWISE ROTATING CHANNEL

Sedat Tardu and **Julien Barenzung**
Laboratoire des Ecoulements Géophysiques et Industriels (LEGI)
B.P. 53 X 38041 Grenoble, Cédex, France
Sedat.Tardu@hmg.inpg.fr

ABSTRACT

Development of anisotropy in a spanwise rotating channel is analyzed in time and space through direct numerical simulations. The aim is to understand how the anisotropy sets-up both in time and space in a supercritical flow, the role of rotation being rather generic in this particular context. Several techniques to quantify anisotropy are used such as the trajectories in time and space of the Lumley invariants, the dissipation tensor invariants and local anisotropy characterization in spectral domain. It is shown that large excursions within the Lumley triangle occur near the centerline, and the local perturbation hesitates for long time between a one component to a nearly isotropic state. The wall damps these excursions; the local turbulence structure changes only slightly near the wall and it remains basically axisymmetric.

INTRODUCTION

Investigating the response of the forced wall turbulence is difficult because, it is generally hard to identify a turbulent structure, isolate it from its rush environment and track it in time and space. Furthermore, the interaction of the given structure with its incoherent surrounding renders the analysis delicate. The strategy to resolve this problem, at least partially, is to proceed by a by-pass like method, i.e. to inject an individual structure in a supercritical flow and determine its development in time and space, until it leads to a fully developed turbulence. That is the methodology adopted here with the main aim to study how a structure with a given initial anisotropy characteristics respond to the structural changes and how the anisotropy develops in time and space. A supercritical spanwise rotating channel flow is chosen as the generic case for this purpose. Different methods to identify the anisotropy both in physical and spectral domains are subsequently used and analyzed.

BASE FLOW CONFIGURATION

A local perturbation in the form of a quasi-streamwise pair of vortices is followed in time and space, in a way quite similar to the investigations dealing with by-pass transition (Henningson et al., 1993). The perturbation takes rapidly the form of a local turbulent spot as it is seen in Fig.1 for Rossby and Reynolds numbers that are respectively $Ro = U_c / 2\Omega h = 6$, and $Re = U_c h/\nu = 1500$ (here Ω is the angular rotation velocity, U_c is the centerline velocity, h is the channel half width and ν is the viscosity). Hereafter, the flow quantities are scaled by h and U_c. Direct numerical simulations are used for this purpose. The computational domain extends to $16\pi h \times 2h \times 8\pi h$ in the streamwise, wall normal and spanwise directions and the number of computational modes are respectively $256 \times 128 \times 256$. Stretched coordinates are used in the wall normal direction. The critical Reynolds number under these circumstances is $Re_c = 150$ according to (Alfredsson and Persson, 1989) and the flow is supercritical here. The perturbation becomes a developed turbulent spot before it leaves the computational domain. For this reason, the rotation is rather generic in this investigation allowing the time tracking of the local spot from its early until its developed stages. A similar analysis in the canonical channel flow without rotation would require a much longer computational domain and/or a stronger initial perturbation. We could determine the frontiers of the developing perturbation simply by sweeping the instantaneous vorticity field through a threshold method, in the homogeneous y planes (x,y and z are respectively the longitudinal, wall normal and spanwise directions, with u,v and w being the corresponding fluctuating velocity components-in the indicial notations we use x_i and u_i where $i = 1,2$ and 3 correspond in order to x,y and z, idem for the velocity field). The flow indeed becomes fully developed turbulent as early as at $t = 240$ as it is seen in Fig. 2 that shows the distribution of the longitudinal $u' = \sqrt{\overline{uu}}$, wall normal $v' = \sqrt{\overline{vv}}$ and spanwise $w' = \sqrt{\overline{ww}}$ turbulent intensity scaled by the arithmetic mean of the pressure-suction sides wall shear stress. The classical reaction of the wall turbulence under spanwise rotation is observed in Fig. 2a, with the wall activity increasing at the pressure side.

The shear stress tensor is defined as usual by

$$b_{ij} = \frac{\overline{u_i u_j}}{\overline{u_k u_k}} - \frac{1}{3}\delta_{ij} \quad (1)$$

where u_i is the fluctuating velocity component and δ_{ij} is the Kronecker symbol (Simonsen and Krogstad, 2005). Fig. 2b shows the classical Lumley chart in the fully developed rotating channel. The turbulence near the wall develops along the 2 component line of the –II and III invariants. It approaches a rod-like axisymmetric form further away from the wall and local isotropy near the centerline, but does not entirely reach this state, in contrast with canonical turbulent wall flows without rotation in which the turbulence travels very near the rod-like line.

RESULTS

The initial perturbation is a pair of counterrotaing vortices generated by the streamfunction:

$$\psi = \varepsilon f(y)\left(x'/l_x\right) z' \exp\left[-\left(x'/l_x\right)^2 - \left(z'/l_z\right)^2\right] \quad (2)$$

where

$$f(y) = (1+y)^p (1-y)^q, p = q = 2, \varepsilon = 0.1, l_x = l_z = 4 \quad (3)$$

We could determine the frontiers of the developing perturbation simply by sweeping the instantaneous vorticity field through a threshold method, in the homogeneous y planes and the results were satisfactory (not shown here). Most of the quantities, especially the invariants of the dissipation tensor have been computed within the perturbation volume.

The trajectories in the Lumley chart have been followed in time in the homogeneous y planes. It was noticed that near the centerline, the local perturbation "hesitates" for a while between a 2 component and a rod-like axisymmetric structural form along which it finally continues its journey before reaching an "equilibrium" state. The transformation from one component to a nearly isotropic state takes time in this region. This behavior is common in the part of the flow that would correspond to the "external" layer in a fully developed turbulent rotating channel flow. Large excursions within the Lumley triangle also occur in the intermediate zone $-0.8 \le y \le -0.5$ with turnovers upon 2 component to rod-like structures. Beginning from $y = -0.8$, i.e. in the inner layer in return, there is no such *hesitation,* and the excursions take place along 2 component to one component axisymmetric line. Fig. 3 shows the excursions of the –II invariant at respectively very close to the wall $y/h = -0.99$ and in the "outer" layer at $y/h = -0.1$. The reader can notice that the trajectories at the wall closely follow the 2 component line, while they are somewhat more chaotic, near the centerline.

Fig. 4 shows the time variations of the invariants –II and III of the shear stress tensor at respectively the channel centerline $y = 0$ and near the wall at $y = -0.95$ (the lower wall is at $y = -1$). The time oscillations of the invariants seen in Fig. 4 are strongly nonlinear near the centerline, while there is a clear effect of damping near the wall. A closer look to the data revealed that the temporal response of the shear stress tensor invariants could be modeled as a Duffing non-linear oscillator with damping increasing towards the wall (not shown here).

The response of the dissipation tensor invariants is qualitatively similar, yet there are quantitative differences in their temporal variations compared with the shear stress invariants. Recall that the dissipation tensor is defined as

$$d_{ij} = \frac{\varepsilon_{ij}}{2\varepsilon_K} - \frac{\delta_{ij}}{3} \quad (4)$$

wherein the dissipation tensor and its contraction ε_K are

$$\varepsilon_{ij} = 2\nu \overline{\frac{\partial u_i}{\partial x_k}\frac{\partial u_j}{\partial x_k}}, \text{ and } \varepsilon_K = \sum_{i=1}^{3} \varepsilon_{ii}/2 \quad (5)$$

The reaction of the invariants related to d_{ij} are similar to b_{ij} at least qualitatively. The damping effect of the wall is once more clear from in Fig. 5a that shows the behavior of the invariant II at $y/h = -0.99$: the trajectories follow the 2 component axisymmetric- 1 component line, without penetrating into the triangle. The structure of turbulence changes only slightly and remains basically axisymmetric. Large excursions within the triangle take place as one goes further into the flow (Fig. 5b) and the time spent into the triangle increases as one approaches the outer layer. The trajectories become more and more irregular as one approaches further the centerline. Turbulence hesitates to become isotropic. The passage from nearly one-component to (nearly) isotropic state takes time.

It is possible in canonical (non rotating) wall turbulence to approximate the shear tensor b_{ij} by using an algebraic equation for d_{ij} which is typically of the form

$$b_{ij}\left(y^+\right) \propto c\left(y_c^+\right) d_{ij}\left(y_c^+\right) \quad (6)$$

where

$$y_c^+ = f\left(y^+\right) \quad (7)$$

is a function of the distance to the wall in wall units. Such a relationship is also plausible in rotating turbulence. We compare the tensors b_{ij} and d_{ij} in Fig. 6 at $t = 240$ at which time the flow is fully developed. It is seen that the dissipation tensor invariants follow better the borders of the Lumley triangle compared to b_{ij}, and that large differences between b_{ij} and d_{ij} persist near the (pseudo isotropic) centerline.

We determined the *velocity* distribution of the trajectories into the Lumley triangle to provide quantitative information concerning the set-up of anisotropy. The results will not be detailed in this short paper and will be published elsewhere. We noticed that the velocity decreases linearly in time as expected, with large dispersion along the constant acceleration line. There is no clear dependence upon the distance from the wall.

The local isotropy of high and low frequency structures has been determined by computing the modulus of Fourier transforms of local shear stresses in the homogeneous planes and by determining the invariants of the related normalized tensor in a way much similar to Liu and Pletcher (2008). The local anisotropy of high and low frequency structures has been determined by computing

$$\psi_{ij}\left(t;y,\kappa_x,\kappa_z\right)=\frac{4\pi^2}{L_xL_z}\int_0^{L_x}\int_0^{L_z}u'_iu'_j\left(t,y,x,z\right)\exp\left[-2\pi i\left(\frac{x\kappa_x}{L_x}+\frac{z\kappa_z}{L_z}\right)\right]dx\,dz \tag{8}$$

The Fourier transform is computed at homogeneous (x,z) planes at a given distance y from the wall. Let us denote by F_{ij} the amplitude of ψ_{ij}. We define the tensor

$$\mathbf{A}=\frac{F_{ij}\left(t;y,\kappa_x,\kappa_z\right)-F_{kk}\left(t;y,\kappa_x,\kappa_z\right)\frac{\delta_{ij}}{3}}{F_{kk}\left(t;y,\kappa_x,\kappa_z\right)} \tag{9}$$

where $F_{kk}\left(t;y,\kappa_x,\kappa_z\right)$ is related to the amplitude of the kinetic energy Fourier transform. The invariants of $\mathbf{A}$ describe the local anisotropy in the spectral domain. The procedure is much similar to that used in Liu and Pletcher (2008). Fig. 7 shows the distribution of the second invariant of $\mathbf{A}$ at a given distance from the wall and time in the Fourier plane (κ_x,κ_z). The second invariant is highly intermittent, *granular* and clearly appears as multi-fractal. This is not the case for $Ro=\infty$. These results will be discussed in more details in the symposium. The small-scale singularities observed in the invariants diluted rapidly in space as the time was increased, but the high intermittency and the granular geometry persisted even at large development times. There are no apparent preferential direction or concentration zones in the spectral domain. Indeed, we computed the "center of gravity" of the spectral invariants in the (κ_x,κ_z) plane at different y/h positions, and did not notice significant differences (not shown here).

We first computed the time average of the spectral invariants $\overline{II}$ and $\overline{III}$ at large developing times (between $t=120$ and $t=240$) and then averaged the time mean invariants in the spanwise wavenumber range through

$$\iota_{II}=-\frac{1}{L_z}\int_0^{L_z}\overline{II}\,dk_z \text{ and } \iota_{III}=\frac{1}{L_z}\int_0^{L_z}\overline{III}\,dk_z \tag{10}$$

at several y/h. The corresponding distributions are shown in Fig. 8. It is seen that in the high frequency range at typically $k_x\geq 20$ both ι_{II} and ι_{III} are independent of y/h. That means that small scale structures have the same local anisotropy across the entire layer in the fully developed regime. At small values of the wavenumber $k_x\leq 10$, the spanwise averaged mean local anisotropy is larger near the centreline, than near the wall. For instance $\iota_{II}=0.8$ at $y/h=0$ that is larger than $\iota_{II}=0.6$ at $y/h\leq -0.7$. The tendency observed in the ι_{III} distribution is similar. That surprisingly indicates that large scale structures are (slightly) more anisotropic in the outer layer than in the inner layer. Another interpretation might be that the repercussion of the large scale structures on the anisotropy is less significant in the inner than the outer-layer. Given that it is difficult to assess strongly anisotropic large-scale structures in the outer layer, the second interpretation seems to be more plausible. Note finally that these behaviours are similar to those observed in a canonical turbulent boundary layer (Liu and Pletcher, 2008).

CONCLUSION

The development of a local perturbation is analyzed in a subcritical spanwise rotating channel flow, with the aim to determine how the anisotropy involves in time and space. The time-space tracking of invariants of the shear stress and dissipation tensors shows that the local disturbance hardly reaches its isotropic state near the centreline. The time response of the shear stress invariants is strongly non linear in the outer layer. The trajectories of the invariants within the Lumley triangle follow basically the axisymmetric line near the wall whose strong damping effect results in rather smooth temporal variations. The observed behaviors can be modeled through a non-linear Duffing oscillator whose damping coefficient increases progressively from the centreline to the wall.

REFERENCES

Alfredsson P.H. and Persson H. : Instabilities in channel flow with system rotation, J. Fluid Mech., Vol. 202, pp. 543-557 (1989).

Henningson D.S., Lundbladh A., Johansson A.V. :A mechanism for bypass transition from localized disturbances in wall-bounded shear flows, J. Fluid Mech., Vol. 250, pp. 169-207 (1993).

Liu K, Pletcher R.H. :Anisotropy of a turbulent boundary layer, Journal of Turbulence, Vol. 9 (18), pp. 1-18 (2008).

Simonsen A.J., Krogstad P.A. : Turbulent stress invariant. Clarification of existing terminology. Phys. Fluids, Vol. 17, 088103 (2005).

ACKNOWLEDGMENTS

We are grateful to IDRIS (Institut de développement et des resources en informatique scientifique) of the National Research Center CNRS, for their continuous support.

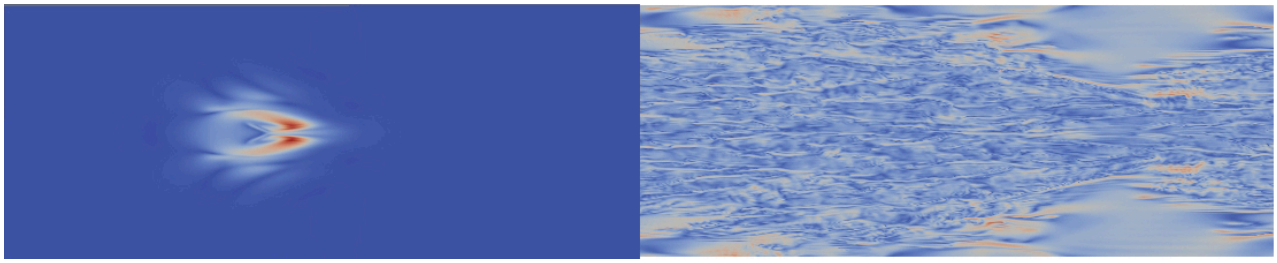

Figure 1. Time-space evolution of the localized perturbation at $Ro = 6$ and $Re = 1500$ at $t = 20$ (left) and $t = 110$ (right) in terms of instantaneous turbulence kinetic energy contours.

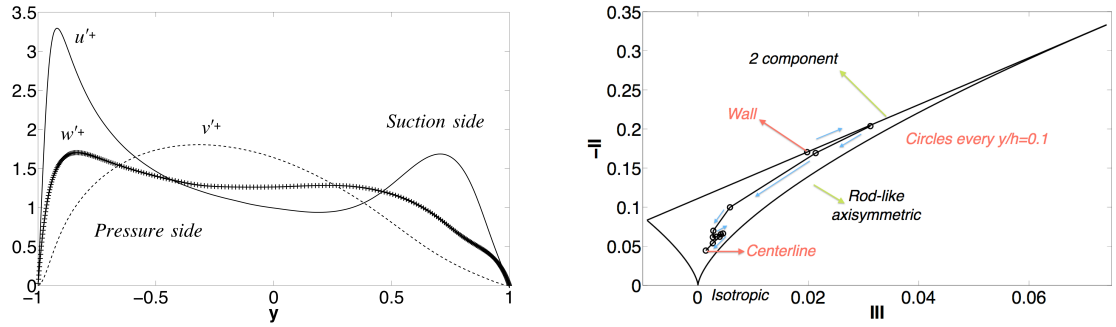

Figure 2. (Left) Turbulent intensity profiles at $t = 240$ in the fully developed turbulent spanwise rotating channel flow ($Ro = 6$ and $Re = 1500$). (Right) Lumley chart in the fully developed turbulent rotating channel.

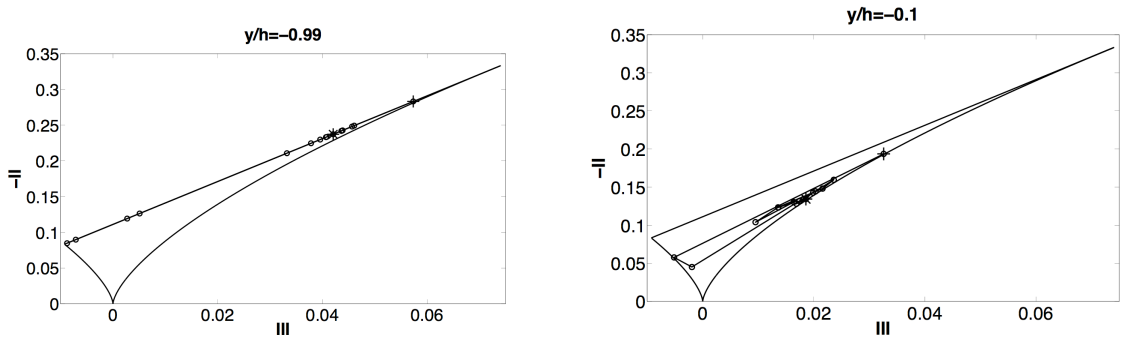

Figure 3. Trajectories of the stress tensor invariants in Lumley triangle near the wall (left) and the centerline (right). Final time is at $t = 240$. + : Departure ; * : Arrival points.

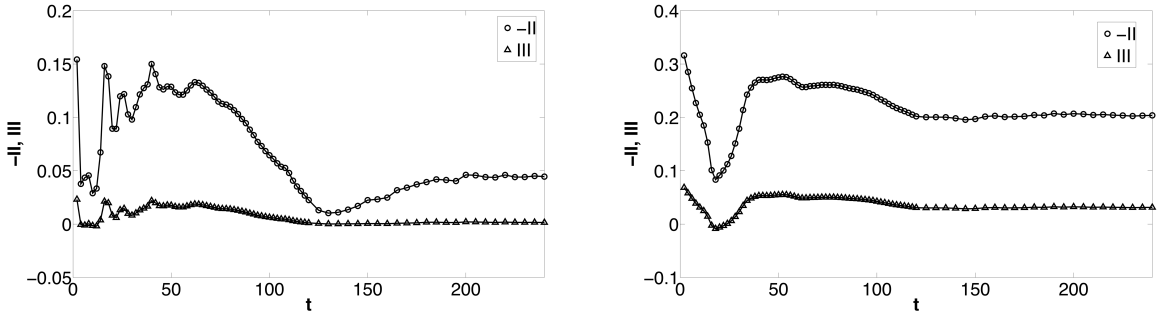

Figure 4. Temporal evolution of the second and third invariants of shear stress tensor at the centerline $y/h = 0$ (left) and near the wall at $y/h = -0.95$ (right).

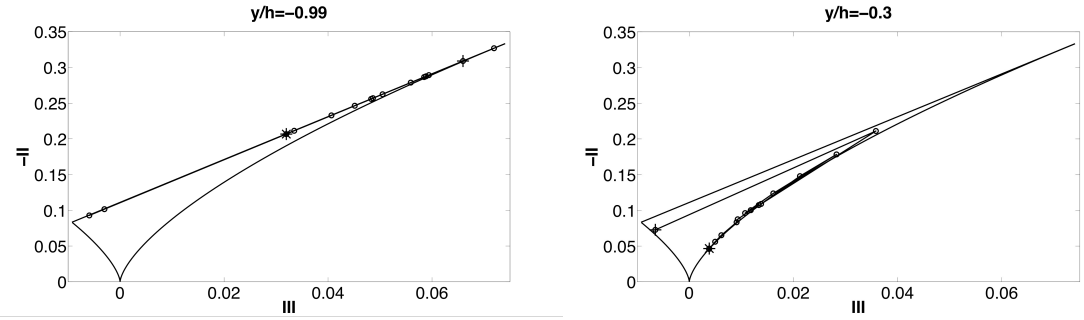

Figure 5. Trajectories of the dissipation tensor invariants in Lumley triangle near the wall (left) and the centerline (right). Final time is at $t = 240$. + : Departure ; * : Arrival points.

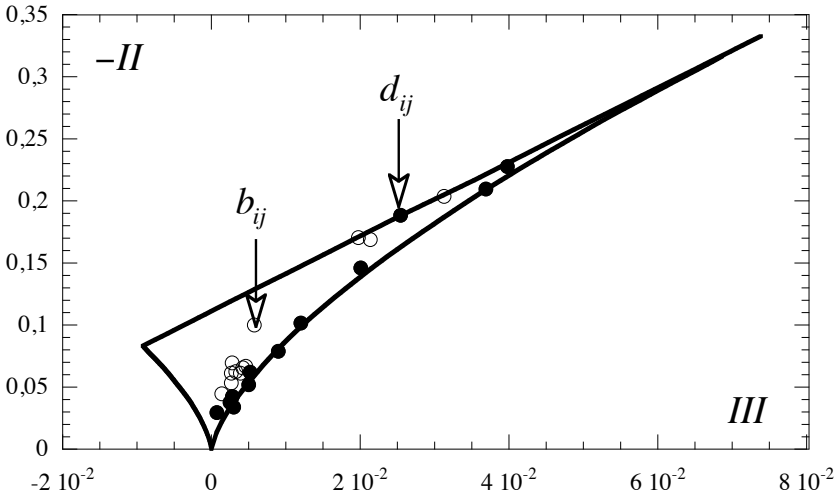

Figure 6. Lumley triangle in the fully developed state at $t = 240$. Open circles correspond to the stress tensor, and closed symbols to the dissipation tensor. Points are shown every $y/h = 0.1$.

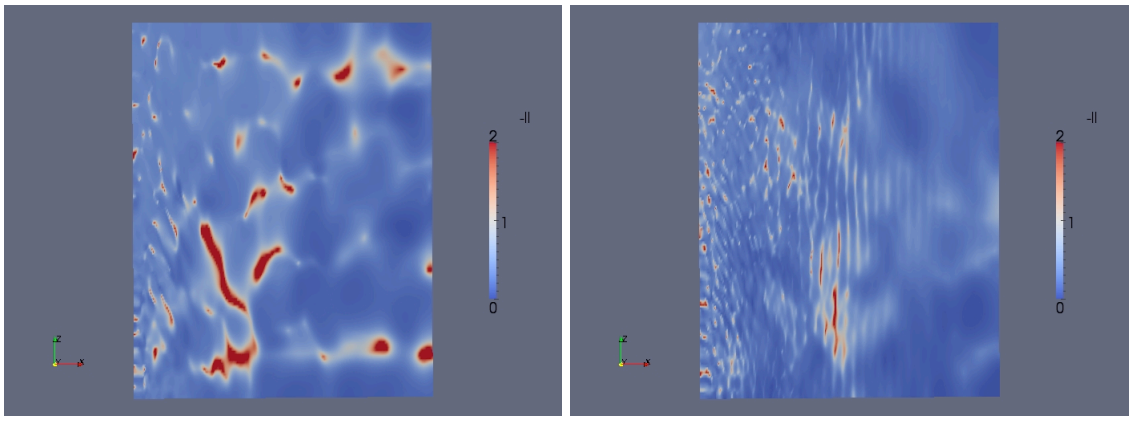

Figure 7. The second invariant of the spectral tensor as defined in the text at $t = 30$. Left $y/h = -0.9$, right $y/h = -0.7$.

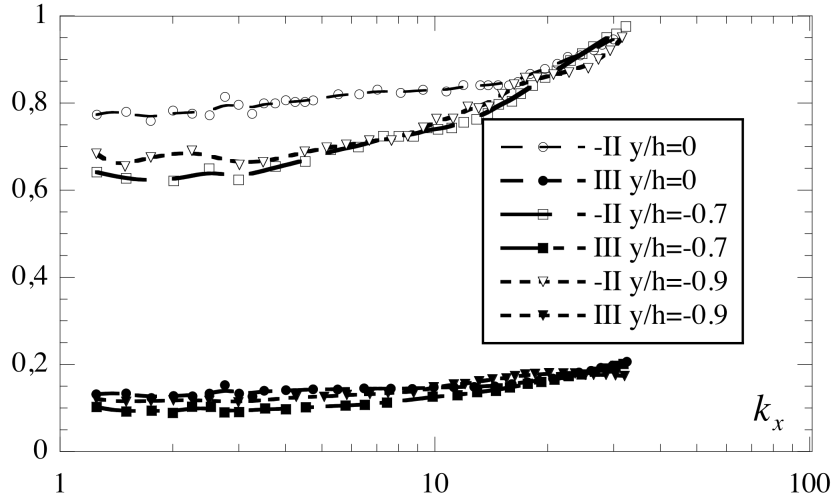

Figure 8. Time mean spanwise averaged local spectral anisotropy $-\frac{1}{L_z}\int_0^{L_z} \overline{II}\, dk_z$ (and $\frac{1}{L_z}\int_0^{L_z} \overline{III}\, dk_z$) versus the streamwise wavenumber (time average performed between t=120 and 240).